Available online at www.sciencedirect.com
ScienceDirect
Journal of Power Sources 163 (2006) 460–466
JOURNAL OF POWER SOURCES
www.elsevier.com/locate/jpowsour

A modeling study on concentration overpotentials of a reversible solid oxide fuel cell

Meng Ni, Michael K.H. Leung *, Dennis Y.C. Leung

Department of Mechanical Engineering, The University of Hong Kong, Pokfulam Road, Hong Kong, PR China

Received 21 July 2006; received in revised form 28 August 2006; accepted 15 September 2006
Available online 27 October 2006

Abstract

A single reversible solid oxide fuel cell (RSOFC) can perform dual functions: (1) as a solid oxide steam electrolyzer (SOSE) for hydrogen production and (2) as a solid oxide fuel cell (SOFC) for power generation. Thus, RSOFC can potentially offer a low-cost approach to support hydrogen economy. A modeling study has been conducted to analyze the important concentration overpotentials in both SOSE and SOFC modes of operation. The quantitative analyses show that in the SOSE mode, the hydrogen electrode is vulnerable to high concentration overpotential and limiting current density. Oppositely, in the SOFC mode, the oxygen electrode is vulnerable to above problems. If the SOSE and SOFC modes are considered separately, a RSOFC should be oxygen-electrode-supported and hydrogen-electrode-supported, respectively. For this reason, comprehensive analysis is very important to optimize the structure of the electrode-support to maximize the overall efficiency of a RSOFC performing dual functions. The modeling study signifies the difference between the SOSE and SOFC modes and provides insights in the operating mechanisms of RSOFC. The present model can be further extended to conduct more simulations for design optimization.

Keywords: Reversible solid oxide fuel cell (RSOFC); Solid oxide steam electrolyzer (SOSE); Dual modes; Concentration overpotentials

1. Introduction

Hydrogen has been identified as an ideal energy carrier to support sustainable energy development. Hydrogen can be effectively produced by reforming fossil fuels, e.g. natural gas steam reforming [1–4]. However, the greenhouse gases produced will harm the environment and fossil fuels will be depleted beyond their economical usage in the foreseeable future. Development of renewable, clean, and economical hydrogen production technologies to replace fossil fuel-based hydrogen production methods is a key step towards a sustainable hydrogen economy [2].

Water electrolyzers integrated with photovoltaics or wind turbines will play an important role in renewable hydrogen production [5]. Among different types of electrolyzers, solid oxide steam electrolyzers (SOSE) are more advantageous due to their high efficiency [6–10]. Recently, the U.S. Department of Energy (DOE) initiated several projects on hydrogen production using SOSE [11–13].

Since, a SOSE has the same electrodes and electrolyte as a solid oxide fuel cell (SOFC) but works in a reverse SOFC process, the concept of reversible solid oxide fuel cell (RSOFC) is feasible. That means a RSOFC can be operated in the SOSE mode to produce hydrogen fuel and the same RSOFC can later consume the hydrogen fuel to generate electricity in the SOFC operating mode [14–19]. The capability of dual functions makes RSOFC economically sound.

In the present literature, some experimental studies on RSOFC are available but there is a lack of detailed modeling studies, which are indeed important for a better understanding of the operating mechanisms as well as for design optimization. Under the same operating condition (i.e., same temperature and same current density), a RSOFC working in either the SOSE or SOFC mode has identical ohmic and activation overpotentials. The overpotentials can be determined by the models reported previously [20–36]. On the other hand, the concentration overpotentials are different between the SOSE and SOFC modes because of the different gas transport mechanisms in the porous electrodes. Therefore, the concentration overpotentials are the sole factor responsible for the different RSOFC current–voltage (J–V) characteristics between the SOSE and SOFC modes. For

* Corresponding author. Tel.: +852 2859 2628; fax: +852 2858 5414.
E-mail address: mkhleung@hku.hk (M.K.H. Leung).

0378-7753/$ – see front matter © 2006 Elsevier B.V. All rights reserved.
doi:10.1016/j.jpowsour.2006.09.024

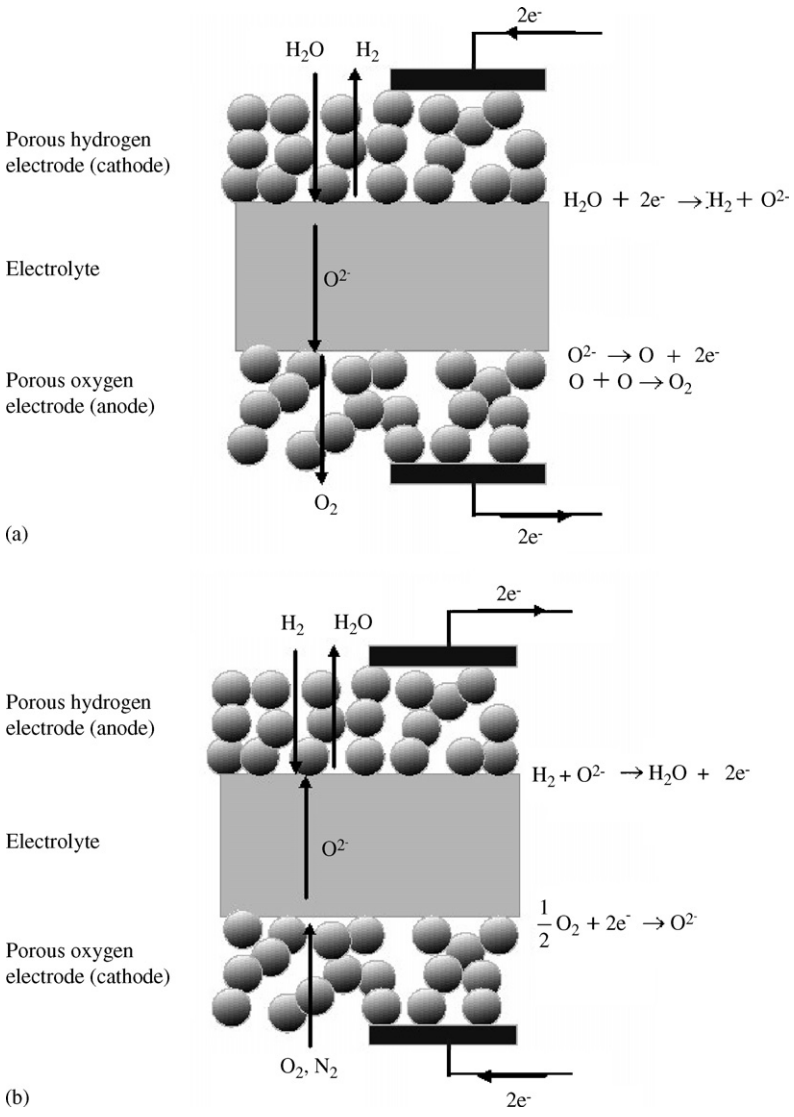

Fig. 1. Operating mechanisms of RSOFC in (a) SOSE mode; and (b) SOFC mode.

this reason, the emphasis of this study is on modeling of the concentration overpotentials of a RSOFC.

2. Model development

2.1. Operating mechanisms

The fundamental mechanisms of a RSOFC working in the SOSE mode are illustrated in Fig. 1a. Steam is fed to the porous hydrogen electrode (cathode). When an electrical potential, sufficient for water-splitting, is applied to the two electrodes, the water molecules diffused to the cathode-electrolyte interface are dissociated into hydrogen gas and oxygen ions. The hydrogen molecules produced are diffused out of the hydrogen electrode. The oxygen ions are transported through the electrolyte to the porous oxygen electrode (anode) and then oxidized to form oxygen molecules. Subsequently, oxygen, being the only substance in the mass transport in the porous oxygen electrode, is driven out by means of permeation. The net SOSE reaction can be expressed as

$$H_2O \rightarrow H_2 + \tfrac{1}{2}O_2. \quad (1)$$

The working mechanisms of RSOFC in the SOFC mode with air as the source of oxidant are illustrated in Fig. 1b. Unlike the SOSE mode, oxygen and nitrogen, instead of pure oxygen, are present in the oxygen electrode. Thus, oxygen is transported by self-diffusion in the SOFC mode [23,24].

2.2. RSOFC cell potentials

The *J–V* characteristics of RSOFC can be evaluated by the cell potentials related to the Nernst potential (E), activation overpotentials (η_{act,H_2} and η_{act,O_2}), ohmic overpotential (η_{ohmic}), and concentration overpotentials (η_{con,H_2} and η_{con,O_2}) in the SOSE mode,

$$V_{SOSE} = E + \eta_{act,H_2} + \eta_{act,O_2} + \eta_{ohmic} + \eta^{SOSE}_{con,H_2} + \eta^{SOSE}_{con,O_2}, \quad (2)$$

and in the SOFC mode,

$$V_{\mathrm{SOFC}} = E - \eta_{\mathrm{act,H_2}} - \eta_{\mathrm{act,O_2}} - \eta_{\mathrm{ohmic}} - \eta^{\mathrm{SOFC}}_{\mathrm{con,H_2}} - \eta^{\mathrm{SOFC}}_{\mathrm{con,O_2}}. \quad (3)$$

The Nernst potential can be determined by the Nernst equation. The activation overpotentials can be determined by the Butler–Volmer equation [17,18]. The ohmic overpotential dependent of the current density, electrolyte thickness, and operating temperature can be obtained by [20]

$$\eta_{\mathrm{ohmic}} = 2.99 \times 10^{-5} JL \exp\left(\frac{10300}{T}\right) \quad (4)$$

where T (K) is absolute temperature and L (μm) is the thickness of the electrolyte.

2.3. Concentration overpotentials in the SOSE mode

The concentration overpotential is caused by the resistance to the transport of reactant species approaching the reaction sites and the transport of product species leaving the reaction sites. In the SOSE mode, the concentration overpotentials can be expressed in terms of the gas concentration difference between the electrode surface and the electrode-electrolyte interface as [23,24,26]

$$\eta^{\mathrm{SOSE}}_{\mathrm{con,H_2}} = \frac{RT}{2F} \ln\left(\frac{P^{\mathrm{I}}_{\mathrm{H_2}} P^{0}_{\mathrm{H_2O}}}{P^{0}_{\mathrm{H_2}} P^{\mathrm{I}}_{\mathrm{H_2O}}}\right) \quad (5)$$

and

$$\eta^{\mathrm{SOSE}}_{\mathrm{con,O_2}} = \frac{RT}{2F} \ln\left[\left(\frac{P^{\mathrm{I}}_{\mathrm{O_2}}}{P^{0}_{\mathrm{O_2}}}\right)^{1/2}\right] \quad (6)$$

where P^0 and P^{I} are the partial pressures at the electrode surface and electrode–electrolyte interface, respectively, and subscripts H_2O, H_2, and O_2 represent the steam reactant, hydrogen and oxygen products, respectively.

It is assumed that the electrochemical reactions take place at the electrode–electrolyte interfaces [23,24]. Each participating component undergoes a steady-state mass transport in the porous electrode [26,40,41],

$$\nabla N_i = 0 \quad (7)$$

where N_i is the rate of mass transfer of species i. In the SOSE porous hydrogen electrode (cathode), the mass transport mechanism is based on diffusion as the gas molar generation rate is equal to gas molar consumption rate. Both Fick's model and Dusty Gas Model (DGM) are frequently used to describe gas transport within porous media. DGM is based on Stefan Maxwell equations and includes Knudsen diffusion. However, no analytical expression can be obtained and numerical method must be employed. In comparison, Fick's model is the simplest model that can describe the gas transport characteristics effectively. Furthermore, analytical solutions can be obtained by using Fick's model. In the present study, the diffusion process, which is driven by concentration gradient or partial pressure gradient, is determined by Fick's model [40],

$$N_i = -\frac{D^{\mathrm{eff}}_i}{RT}\frac{\partial(y_i P)}{\partial x} = -\frac{D^{\mathrm{eff}}_i}{RT}\frac{\partial(P_i)}{\partial x}, \quad i = 1, 2, \ldots \quad (8)$$

where P is the operating pressure, x is the depth measured from the electrode surface, P_i, y_i, and D^{eff}_i are the partial pressure, molar fraction, and effective diffusion coefficient of species i, respectively. Substituting Eq. (8) into Eq. (7), the equation governing the mass transport of species i can be obtained,

$$\frac{\partial}{\partial x}\left[-\frac{D^{\mathrm{eff}}_i}{RT}\frac{\partial(P_i)}{\partial x}\right] = 0 \quad (9)$$

where i represent H_2O and H_2 at the cathode. It is noted that for advanced porous electrodes of which reactions can take place in the porous media, the micromodel developed by Chan and co-workers can be employed [37–39].

At the cathode-electrolyte interface ($x = d_{\mathrm{H_2}}$, the thickness of cathode), the diffusion rate of H_2O towards the interface is equal to the H_2O consumption rate under steady state condition. As H_2O consumption is governed by the electrical current density J, the mass transfer rate can be expressed as

$$N_{\mathrm{H_2O}} = \frac{J}{2F}. \quad (10)$$

Substituting Eq. (10) into Eq. (8), the boundary condition for the governing Eq. (9) becomes

$$\left.\frac{\partial P_{\mathrm{H_2O}}}{\partial x}\right|_{x=d_{\mathrm{H_2}}} = -\frac{J}{2F}\frac{RT}{D^{\mathrm{eff}}_{\mathrm{H_2O}}}. \quad (11)$$

The Dirichlet boundary condition can be applied for the cathode surface,

$$P_{\mathrm{H_2O}}\big|_{x=0} = P^{0}_{\mathrm{H_2O}}. \quad (12)$$

Solving Eq. (9) with the above two boundary conditions, the partial pressure of H_2O at the cathode-electrolyte interface can be obtained,

$$P^{\mathrm{I}}_{\mathrm{H_2O}} = P^{0}_{\mathrm{H_2O}} - \frac{RT}{D^{\mathrm{eff}}_{\mathrm{H_2O}}}\frac{J}{2F}d_{\mathrm{H_2}}. \quad (13)$$

As the steam molar consumption rate is equal to the hydrogen molar generation rate, the cathode total pressure ($P = P_{\mathrm{H_2}} + P_{\mathrm{H_2O}}$) is constant. Therefore,

$$P^{\mathrm{I}}_{\mathrm{H_2}} = P - P^{\mathrm{I}}_{\mathrm{H_2O}} = P - \left(P^{0}_{\mathrm{H_2O}} - \frac{RT}{D^{\mathrm{eff}}_{\mathrm{H_2O}}}\frac{J}{2F}d_{\mathrm{H_2}}\right) = P^{0}_{\mathrm{H_2}} + \frac{RT}{D^{\mathrm{eff}}_{\mathrm{H_2O}}}\frac{J}{2F}d_{\mathrm{H_2}}. \quad (14)$$

Substituting Eqs. (13) and (14) into Eq. (5), the concentration overpotential of the hydrogen electrode can be obtained,

$$\eta^{\mathrm{SOSE}}_{\mathrm{con,H_2}} = \frac{RT}{2F}\ln\left[\frac{P^{0}_{\mathrm{H_2O}}(P^{0}_{\mathrm{H_2}} + (JRTd_{\mathrm{H_2}}/2FD^{\mathrm{eff}}_{\mathrm{H_2O}}))}{P^{0}_{\mathrm{H_2}}(P^{0}_{\mathrm{H_2O}} - (JRTd_{\mathrm{H_2}}/2FD^{\mathrm{eff}}_{\mathrm{H_2O}}))}\right] = \frac{RT}{2F}\ln\left(\frac{1 + (JRTd_{\mathrm{H_2}}/2FD^{\mathrm{eff}}_{\mathrm{H_2O}}P^{0}_{\mathrm{H_2}})}{1 - (JRTd_{\mathrm{H_2}}/2FD^{\mathrm{eff}}_{\mathrm{H_2O}}P^{0}_{\mathrm{H_2O}})}\right). \quad (15)$$

The diffusion in the porous SOSE electrodes is mainly based on two mechanisms, namely, molecular diffusion and Knudsen diffusion. Molecular diffusion is the dominant mechanism if the pore size is much larger than the mean free path of the molecular species. In this case, the molecule–molecule interaction governs the diffusion process. On the other hand, if the pore size is much smaller than the mean free path of the species, the molecule–pore wall interaction dominates over the molecule–molecule interaction. Thus, Knudsen diffusion becomes an important mechanism. In most porous structures, both mechanisms are significant. The effective diffusion coefficient of steam can be expressed by combining these two diffusion mechanisms using the Bosanquet formula [26,40,41],

$$\frac{1}{D^{\text{eff}}_{\text{H}_2\text{O}}} = \frac{\xi}{\varepsilon}\left(\frac{1}{D_{\text{H}_2\text{O}-\text{H}_2}} + \frac{1}{D_{\text{H}_2\text{O},k}}\right) \tag{16}$$

where ξ/ε is the ratio of cathode tortuosity to porosity, $\xi/(\varepsilon D_{\text{H}_2\text{O}-\text{H}_2})$ is the reciprocal of the effective molecular diffusion coefficient for a H_2O–H_2 binary system, and $\xi/(\varepsilon D_{\text{H}_2\text{O},k})$ is the reciprocal of the effective Knudsen diffusion coefficient for steam.

For the Knudsen diffusion, as gas molecules frequently collide with the walls of the pores, the transport of molecules can be modeled using the kinetic theory [26,40,41],

$$D_{\text{H}_2\text{O},k} = \frac{4}{3} r \sqrt{\frac{8RT}{\pi M_{\text{H}_2\text{O}}}} \tag{17}$$

where r is the mean pore radius and $M_{\text{H}_2\text{O}}$ is the molar weight of H_2O (18 g mol^{-1}). The molecular binary diffusion coefficient $D_{\text{H}_2\text{O}-\text{H}_2}$ can be obtained from the Chapman-Enskog theory of ideal gas [41],

$$D_{\text{H}_2\text{O}-\text{H}_2} = 0.00133\left(\frac{1}{M_{\text{H}_2}} + \frac{1}{M_{\text{H}_2\text{O}}}\right)^{1/2} \frac{T^{3/2}}{P\sigma^2_{\text{H}_2\text{O},\text{H}_2}\Omega_{\text{D}}} \tag{18}$$

where M_{H_2} is the molar weight of H_2 (2 g mol^{-1}); $\sigma_{\text{H}_2\text{O},\text{H}_2}$ is the mean characteristic length of species H_2O and H_2, and Ω_{D} is a dimensionless diffusion collision integral. The analytical values of Ω_{D} and $\sigma_{\text{H}_2\text{O},\text{H}_2}$ can be obtained from references [26,41].

At the oxygen electrode (anode), O_2 is the only gas present in the porous electrode layer. The O_2 generated at the electrolyte–anode interface causes a pressure gradient in the porous electrode. Therefore, O_2 is transported in the electrode by permeation, instead of diffusion. Darcy's law is the most widely used model to characterize gas viscous flow in porous media, depending on the gas dynamic viscosity and the porous microstructure. Employing Darcy's law, the oxygen flux can be determined [22,42],

$$N_{\text{O}_2} = -\frac{P_{\text{O}_2} B_{\text{g}}}{RT\mu}\nabla P_{\text{O}_2} \tag{19}$$

where μ is the dynamic viscosity of O_2, which can be determined by sixth-order polynomial functions developed by Todd and Young [43]; and B_{g} is the flow permeability, which can be determined by the Kozeny–Carman relationship as [44,45]

$$B_{\text{g}} = \frac{\varepsilon^3}{72\xi(1-\varepsilon)^2}(2r)^2. \tag{20}$$

Substituting Eq. (19) into Eq. (7), the governing equation for oxygen transport in the porous anode can be obtained as

$$\frac{\partial}{\partial x}\left[-\frac{P_{\text{O}_2} B_{\text{g}}}{RT\mu}\frac{\partial P_{\text{O}_2}}{\partial x}\right] = 0. \tag{21}$$

At the anode–electrolyte interface ($x = d_{\text{O}_2}$, the thickness of anode), the rate of O_2 transporting away from the interface, which equals to the O_2 generation rate under steady state condition, is also governed by the electrical current density,

$$N_{\text{O}_2} = -\frac{J}{4F}. \tag{22}$$

The boundary condition of Eq. (21) for the anode can be obtained as

$$P_{\text{O}_2}\frac{\partial P_{\text{O}_2}}{\partial x}\bigg|_{x=d_{\text{O}_2}} = \frac{JRT\mu}{4FB_{\text{g}}}. \tag{23}$$

The Dirichlet boundary condition can be applied for the anode surface,

$$P_{\text{O}_2}\big|_{x=0} = P^0_{\text{O}_2}. \tag{24}$$

Solving Eq. (21) with boundary conditions expressed in Eqs. (23) and (24), the partial pressure of O_2 at the anode–electrolyte interface can be obtained,

$$P^{\text{I}}_{\text{O}_2} = \sqrt{\left(P^0_{\text{O}_2}\right)^2 + \frac{JRT\mu d_{\text{O}_2}}{2FB_{\text{g}}}}. \tag{25}$$

The anode concentration overpotential can thus, be expressed as

$$\eta^{\text{SOSE}}_{\text{con},\text{O}_2} = \frac{RT}{4F}\ln\left(\frac{\sqrt{\left(P^0_{\text{O}_2}\right)^2 + (JRT\mu d_{\text{O}_2}/2FB_{\text{g}})}}{P^0_{\text{O}_2}}\right) \tag{26}$$

2.4. Concentration overpotential in the SOFC mode

The following modeling equations developed by Chan and co-workers [23,24] can be employed to determine the concentration overpotentials of a SOFC,

$$\eta^{\text{SOFC}}_{\text{con},\text{H}_2} = -\frac{RT}{2F}\ln\left[\frac{(1-(RT/2F))(Jd_{\text{H}_2}/D^{\text{eff}}_{\text{H}_2}P^0_{\text{H}_2})}{(1+(RT/2F))(Jd_{H_2}/D^{\text{eff}}_{\text{H}_2}P^0_{\text{H}_2\text{O}})}\right], \tag{27}$$

$$\eta^{\text{SOFC}}_{\text{con},\text{O}_2} = -\frac{RT}{4F}\ln\left[\frac{(p_{\text{o}}/\delta_{\text{O}_2}) - ((p_{\text{o}}/\delta_{\text{O}_2}) - P^0_{\text{O}_2})\exp\left[(RT/4F)(J\delta_{\text{O}_2}d_{\text{O}_2}/D^{\text{eff}}_{\text{O}_2}p_{\text{o}})\right]}{P^0_{\text{O}_2}}\right], \tag{28}$$

and

$$\delta_{\text{O}_2} = \frac{D^{\text{eff}}_{\text{O}_2,k}}{D^{\text{eff}}_{\text{O}_2,k} + D^{\text{eff}}_{\text{O}_2-\text{N}_2}} \tag{29}$$

where p_o, $D^{eff}_{O_2}$, $D^{eff}_{O_2,k}$, and $D^{eff}_{O_2-N_2}$ are the pressure of the oxygen electrode, effective oxygen diffusion coefficient, effective Knudsen diffusion coefficient of oxygen, and effective oxygen–nitrogen binary diffusion coefficient, respectively. These diffusion coefficients can be determined by the same method described in previous section.

2.5. Computation procedures

The *J–V* relationship of RSOFC operating in the SOSE mode is implicitly formulated by Eqs. (2), (4), (15), and (26). The analytical Butler–Volmer equations from references [17,18] are directly employed to model activation overpotentials. Using *J* as the independent variable, the numerical values of corresponding ohmic overpotential, activation overpotentials, concentration overpotentials, as well as the cell potential can be computed by direct substitution of values into the right-hand side of the equations. For the SOFC mode, the *J–V* relationship can be obtained by the concentration overpotentials expressed by Eqs. (27) and (28) and the cell potential expressed by Eq. (3).

3. Results and discussion

3.1. Model validation

The above model has been derived to determine the *J–V* characteristics of RSOFC performing dual functions. The model for the SOFC mode developed by Chan and co-workers [23,24] is well accepted (Eqs. (27) through (29)); therefore, no validation is needed. On the contrary, the newly developed model for the SOSE mode should be validated by comparison with experimental data. Momma et al.'s experimental work in SOSE hydrogen production has been selected because the laboratory setup and test procedures are clearly reported in the literature and the details can facilitate the theoretical simulation [46]. In Momma et al.'s experiments, the *J–V* characteristics of hydrogen production by electrolyte-supported planar SOSE discs were measured. The electrolyte, cathode, and anode are made of yttria stabilized zirconia (YSZ), nickel-YSZ (Ni-YSZ), and lanthanum strontium manganite (LSM), respectively. The thickness of the electrolyte, cathode, and anode are 1000 μm, 100 μm, and 100 μm, respectively. The tests were conducted under a constant pressure of 1 atm, steam molar fractions between 20 and 60%, and various operating temperatures from 1173 to 1273 K. In the theoretical simulation, the values of the input parameters are summarized in Table 1 [23,24,26]. The effects of operating temperature and current density on cell potential are shown in Fig. 2. Fig. 3 shows the dependence of the cell potential on the steam molar fraction for *J* equal to 2000 Am^{-2} and *T* equal to 1273 K. The cell potential decreases as the steam molar fraction increases. From Figs. 2 and 3, the good agreement between the theoretical simulation results and the experimental data by Momma et al. [46] serves as a thorough validation of the theoretical model for the SOSE mode.

Table 1
Values of input parameters in the present study

Parameter	Value
Operating temperature, *T* (K)	1073
Operating pressure, *P* (atm)	1.0
Exchange current density at the hydrogen electrode (A/m^2)	5300
Exchange current density at the oxygen electrode (A/m^2)	2000
Electrode porosity, ε	0.3
Electrode tortuosity, ξ	6.0
Average electrode pore radius, *r* (μm)	0.5
Electrolyte thickness, *L* (μm)	1000
Electrode thickness, *d* (μm)	
For model validation	100
For parametric analyses	50, 500

3.2. Concentration overpotentials of hydrogen electrode

Based on a parametric modeling analysis, the concentration overpotentials of the RSOFC hydrogen electrode operated in both SOSE and SOFC modes are compared in Fig. 4. The results

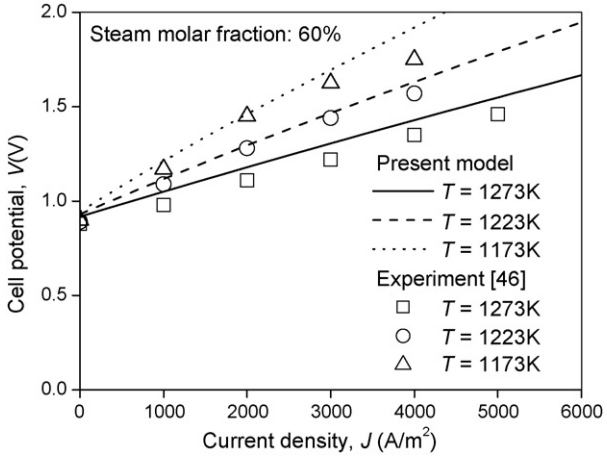

Fig. 2. Comparison of simulation results with experimental data [46] for model validation–effect of operating temperature and current density on RSOFC potential in SOSE mode.

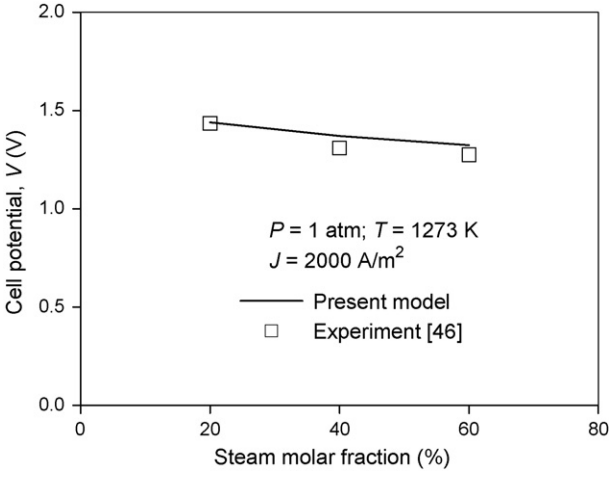

Fig. 3. Comparison of simulation results with experimental data [46] for model validation–effect of steam molar fraction on RSOFC potential in SOSE mode.

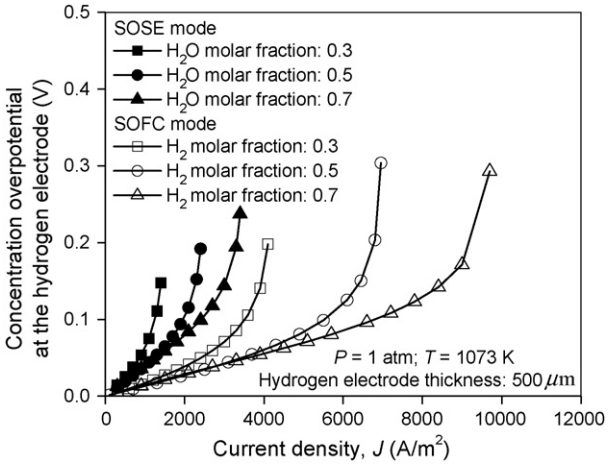

Fig. 4. Comparison of SOSE mode with SOFC mode: concentration overpotentials of hydrogen electrodes.

generally show that the concentration overpotential decreases with increasing reactant gas molar fraction, i.e. H_2O for SOSE and H_2 for SOFC. This finding is consistent with the previous studies that higher cell potential can be achieved by increasing hydrogen molar ratio at the inlet of a SOFC [26]. It is also found that the RSOFC hydrogen electrode has higher concentration overpotential in the SOSE mode than in the SOFC mode. The limiting current density in the SOSE mode is generally lower than that in the SOFC mode. These phenomena can be explained by the diffusion of reactant gases in the porous hydrogen electrode. As H_2O has much higher molecular weight than H_2, the Knudsen diffusion coefficient of H_2O is smaller than that of H_2. Consequently, the RSOFC has a smaller effective diffusion coefficient in the SOSE mode than in the SOFC mode (see Eqs. (16) and (17)). The SOSE concentration overpotential of the hydrogen electrode becomes a more crucial limiting factor.

3.3. Concentration overpotentials of oxygen electrode

Fig. 5 compares the oxygen-electrode concentration overpotentials between the SOSE and SOFC modes. It is found that the difference between the SOSE and SOFC concentration overpotentials is insignificant at low current density below 1400 A/m^2. As the current density increases, the SOSE concentration overpotential increases moderately while the SOFC concentration overpotential increases considerably resulting in a limiting current density.

The SOFC limiting current density occurs because the diffusion rate of reactant O_2 in the porous oxygen electrode is reaching the limit as the O_2 concentration at the oxygen-electrode–electrolyte interface is approaching zero at high current density [23,24]. The low diffusion coefficient due to high molecular weights of O_2 and N_2 yields low effective diffusion coefficient and thus, a low limiting current density. On the other hand, there is no limiting density current for the oxygen electrode in the SOSE mode of operation because the transport of oxygen ions (reactant) through the ion-conducting electrolyte is not limited by the porous electrode.

3.4. Electrode-supported RSOFC

The concentration overpotentials of SOFC have been extensively investigated. It is found that hydrogen-electrode supports, generally more advantageous than oxygen-electrode supports, yield low overpotential loss and high power output [23,24]. This finding is certainly applicable to RSOFC operating in the SOFC mode.

The concentration overpotentials of RSOFC operating in the SOSE mode are studied here in detail with the present theoretical model. In practice, a cell consists of a thick layer of electrode (typically 500 μm) that can provide structural support, while the other electrode is a thin layer (50 μm) to minimize overpotential loss. The characteristics of different electrodes (thick or thin, hydrogen- or oxygen-) are shown in Fig. 6. A thick hydrogen electrode suffers seriously from high concentration overpotential and low limiting current density. For the oxygen electrode, a thick layer only causes a slight increase in the concentration overpotential. More importantly, the oxygen electrode in the SOSE mode does not suffer from limiting current density. The results imply that an oxygen electrode-support performs better than a hydrogen electrode-support in the SOSE mode.

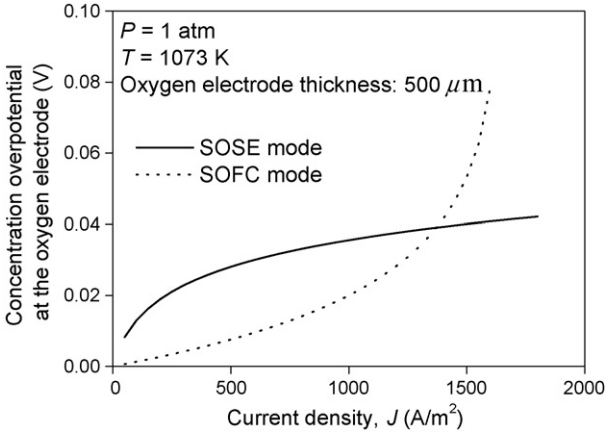

Fig. 5. Concentration overpotentials of oxygen electrodes of RSOFC: SOSE mode vs. SOFC mode.

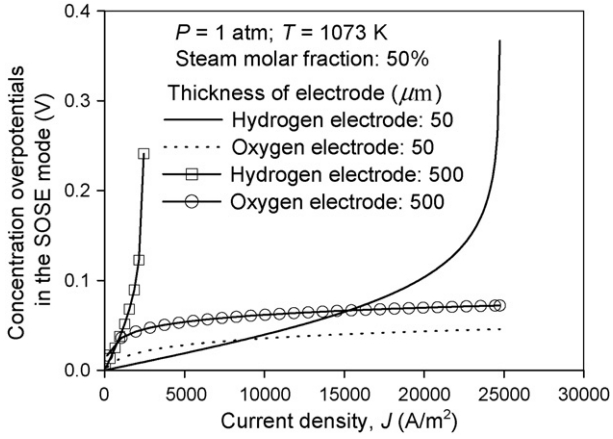

Fig. 6. Concentration overpotentials of RSOFC electrodes in SOSE mode.

Based on the above findings, the selection of an electrode support can greatly affect the overall performance of a RSOFC. A hydrogen-electrode support is favorable to the SOFC mode while an oxygen-electrode support is favorable to the SOSE mode. Therefore, the details of both SOSE and SOFC operating conditions should be carefully considered in design of RSOFC on a case-by-case basis. For example, if a RSOFC is specified mainly to generate high electricity, a hydrogen-electrode support should be chosen in the preliminary design. On the contrary, if a RSOFC is mainly used for hydrogen generation, an oxygen-electrode support is recommended.

4. Conclusion

A theoretical model has been successfully developed to investigate the concentration overpotentials of a RSOFC, which can perform dual functions as a SOSE for hydrogen production and as a SOFC for power generation using hydrogen fuel. The analytical results signify the difference between the SOSE and SOFC operating modes due to different gas transport mechanisms. The theoretical model provides insights of the RSOFC operations. The model can also be effectively applied to subsequent optimization of the RSOFC design for maximum overall energy efficiency.

Acknowledgement

The work described in this paper was part of an ongoing project supported by a grant from the Research Grants Council of Hong Kong, PR China (HKU7150/05E).

References

[1] J.M. Bae, S. Ahmed, R. Kumar, E. Doss, J. Power Sources 139 (2005) 91–95.
[2] W.G. Colella, M.Z. Jacobson, D.M. Golden, J. Power Sources 150 (2005) 150–181.
[3] C.P. Huang, A. T-Raissi, J. Power Sources, doi:10.1016/j.jpowsour.2006.02.082, in press.
[4] A. Ersoz, H. Olgun, S. Ozdogan, J. Power Sources 154 (2006) 67–73.
[5] M. Ni, M.K.H. Leung, K. Sumathy, D.Y.C. Leung, Int. J. Hydrogen Energy 31 (2006) 1401–1412.
[6] M. Ni, M.K.H. Leung, D.Y.C. Leung, Proceedings of the 16th World Hydrogen Energy Conference (WHEC16), Lyon, France, 13–16 June 2006.
[7] R. Hino, K. Haga, H. Aita, K. Sekita, Nucl. Eng. Des. 233 (2004) 363–375.
[8] M. Ni, M.K.H. Leung, D.Y.C. Leung, Chem. Eng. Technol. 29 (2006) 636–642.
[9] B. Yildiz, M.S. Kazimi, Int. J. Hydrogen Energy 31 (2006) 77–92.
[10] V. Utgikar, T. Thiesen, Int. J. Hydrogen Energy 31 (2006) 939–944.
[11] J.A. Ruud, DOE Hydrogen Program, FY 2005 Progress Report, U.S.A., 2005, pp. 361–362.
[12] I.I. Balachov, S. Crouch-Baker, M. Hornbosted, M. McKubre, A. Sanjurjo, F. Tanzella, DOE Hydrogen Program, FY 2005 Progress Report, U.S.A., 2005, pp. 363–366.
[13] J. Hartvigsen, D. Swank, C. Schade, R. Bordia, DOE Hydrogen Program, FY 2005 Progress Report, U.S.A., 2005, pp. 367–369.
[14] O.A. Marina, G.W. Coffev, C.D. Nguyen, E.C. Thomsen, L.R. Pederson, Proceedings of the 208th Meeting of The Electrochemical Society, Los Angeles, CA, United States, 16–21 October, 2005.
[15] H. Uchida, N. Osada, S. Suzuki, M. Watanabe, Proceedings of the 9th International Symposium on Solid Oxide Fuel Cells, SOFC IX, Que., Canada, 15–20 May, 2005.
[16] T. Matsui, A. Ozaki, R. Kikuchi, K. Eguchi, Proceedings of the 9th International Symposium on Solid Oxide Fuel Cells, SOFC IX, Que., Canada, 15–20 May, 2005.
[17] J.A. Ruud, DOE Hydrogen Program, FY 2005 Progress Report.
[18] J. Guan, B. Ramamurthi, J. Ruud, J. Hong, P. Riley, N. Minh, DOE Hydrogen Program Review, Arlington, Virginia, United States, 16–19 May, 2006.
[19] A.V. Virkar, G. Tao, Proceedings of the 209th ECS meeting, Denver, United States, 7–12 May, 2006.
[20] J.R. Ferguson, J.M. Fiard, R. Herbin, J. Power Sources 58 (1996) 109–122.
[21] R.J. Boersma, N.M. Sammes, J. Power Sources 66 (1996) 41–45.
[22] H. Yakabe, M. Hishinuma, M. Uratani, Y. Matsuzaki, I. Yasuda, J. Power Sources 86 (2000) 423–431.
[23] S.H. Chan, K.A. Khor, Z.T. Xia, J. Power Sources 93 (2001) 130–140.
[24] S.H. Chan, Z.T. Xia, J. Appl. Electrochem. 32 (2002) 339–347.
[25] H.Y. Zhu, R.J. Kee, J. Power Sources 117 (2003) 61–74.
[26] E. Hernandez-Pacheco, D. Singh, P.N. Hutton, N. Patel, M.D. Mann, J. Power Sources 138 (2004) 174–186.
[27] Y.X. Lu, L. Schaefer, P.W. Li, J. Power Sources 140 (2005) 331–339.
[28] X. Xue, J. Tang, N. Sammes, Y. Du, J. Power Sources 142 (2005) 211–222.
[29] T.W. Song, J.L. Sohn, J.H. Kim, T.S. Kim, S.T. Ro, K. Suzuki, J. Power Sources 142 (2005) 30–42.
[30] J.J. Hwang, C.K. Chen, D.Y. Lai, J. Power Sources 143 (2005) 75–83.
[31] Y.T. Qi, B. Huang, K.T. Chuang, J. Power Sources 150 (2005) 32–47.
[32] D.A. Noren, M.A. Hoffman, J. Power Sources 152 (2005) 175–181.
[33] R. Suwanwarangkul, E. Croiset, M.D. Pritzker, M.W. Fowler, P.L. Douglas, E. Entchev, J. Power Sources 154 (2006) 74–85.
[34] E.S. Greene, W.K.S. Chiu, M.G. Medeiros, J. Power Sources 161 (2006) 225–231.
[35] A. Smirnov, A. Burt, I. Celik, J. Power Sources 158 (2006) 295–302.
[36] R. Suwanwarangkul, E. Croiset, M.W. Fowler, P.L. Douglas, E. Entchev, M.A. Douglas, J. Power Sources 122 (2003) 9–18.
[37] S.H. Chan, Z.T. Xia, J. Electrochem. Soc. 148 (2001) A388–A394.
[38] S.H. Chan, X.J. Chen, K.A. Khor, J. Electrochem. Soc. 151 (2004) A164–A172.
[39] Z.T. Xia, S.H. Chan, K.A. Khor, Electrochem. Solid State Lett. 7 (2004) A63–A65.
[40] J.W. Veldsink, R.M.J. van Damme, G.F. Versteeg, W.P.M. van Swaajj, Chem. Eng. J. 57 (1995) 115–125.
[41] R.C. Reid, J.M. Prausnitz, B.E. Poling, The Properties of Gases and Liquids, fourth ed., McGraw Hill Book Company, 1987.
[42] D.H. Jeon, J.H. Nam, C.J. Kim, J. Electrochem. Soc. 153 (2006) A406–A417.
[43] B. Todd, J.B. Young, J. Power Sources 110 (2002) 186–200.
[44] H.Y. Zhu, R.J. Kee, V.M. Janardhanan, O. Deutschmann, D.G. Goodwin, J. Electrochem. Soc. 152 (2005) A2427–A2440.
[45] J.H. Nam, D.H. Jeon, Electrochim. Acta 51 (2006) 3446–3460.
[46] A. Momma, T. Kato, Y. Kaga, S. Nagata, J. Ceram. Soc. Jpn. 105 (1997) 369–373.